

1 **Influence of spatial dipole pattern in Asian aerosol changes on East**

2 **Asian summer monsoon**

3

4

5

6 Chao Liu<sup>1</sup>, Yang Yang<sup>1\*</sup>, Hailong Wang<sup>2</sup>, Lili Ren<sup>1</sup>, Jiangfeng Wei<sup>3</sup>, Pinya Wang<sup>1</sup>,

7

Hong Liao<sup>1</sup>

8

9

10

11

12

13

14 <sup>1</sup>Jiangsu Key Laboratory of Atmospheric Environment Monitoring and Pollution

15 Control, Jiangsu Collaborative Innovation Center of Atmospheric Environment and

16 Equipment Technology, School of Environmental Science and Engineering, Nanjing

17 University of Information Science and Technology, Nanjing, Jiangsu, China

18 <sup>2</sup>Atmospheric Sciences and Global Change Division, Pacific Northwest National

19 Laboratory, Richland, Washington, USA

20 <sup>3</sup>School of Atmospheric Sciences, Nanjing University of Information Science and

21 Technology, Nanjing, Jiangsu, China

22

23

24

25

26 \*Correspondence to yang.yang@nuist.edu.cn

27 **Abstract**

28 Since China implemented the air pollution prevention and control action in 2013,  
29 the aerosol emissions in East Asia have been greatly reduced, while emissions in South  
30 Asia have continued to increase. This has led to a dipole pattern of aerosol emissions  
31 between South Asia and East Asia. Here, the East Asian summer monsoon (EASM)  
32 responses to the dipole changes in aerosol emissions during 2013–2017 are investigated  
33 using the atmosphere model of Community Earth System Model version 2 (CESM2).  
34 We show that decreases in East Asian emissions alone lead to a positive aerosol  
35 effective radiative forcing (ERF) of  $1.59 (\pm 0.97) \text{ W m}^{-2}$  over central-eastern China  
36 ( $25^{\circ}$ – $40^{\circ}$ N,  $105^{\circ}$ – $122.5^{\circ}$ E), along with a  $0.09 (\pm 0.07) ^{\circ}\text{C}$  warming in summer during  
37 2013–2017. The warming intensified the land-sea thermal contrast and increased the  
38 rainfall by  $0.32 (\pm 0.16) \text{ mm day}^{-1}$ . When considering both the emission reductions in  
39 East Asia and increases in South Asia, the ERF is increased to  $3.39 (\pm 0.89) \text{ W m}^{-2}$ , along  
40 with an enhanced warming of  $0.20 (\pm 0.08) ^{\circ}\text{C}$  over central-eastern China, while the  
41 rainfall insignificant decreased by  $0.07 (\pm 0.16) \text{ mm day}^{-1}$ . It is due to the westward shift  
42 of the strengthened western Pacific subtropical high, linked to the increase in black  
43 carbon in South Asia. Based on multiple EASM indices, the reductions in aerosol  
44 emissions from East Asia alone increased the EASM strength by almost 5%.  
45 Considering the effect of westward shift of WPSH, the dipole changes in emissions  
46 together increased the EASM by 5–15% during 2013–2017, revealing an important role  
47 of South Asian aerosols in changing the East Asian climate.

## 48 **1. Introduction**

49 Anthropogenic emissions of aerosols and their precursors have increased  
50 significantly since the preindustrial era, especially in East Asia and South Asia due to  
51 industrialization and urbanization (Zhang et al., 2012). As a result of the increase in  
52 emissions, particle pollution has been a big concern over these regions. To mitigate the  
53 air pollution, the Chinese government issued and implemented the air pollution  
54 prevention and control action plan in 2013 and consequently the anthropogenic aerosol  
55 (AA) emissions have been greatly reduced in East Asia (Zheng et al., 2018). Meanwhile,  
56 AA emissions in South Asia are continually increasing, which leads to a spatial dipole  
57 pattern of AA emission changes over the broad continental region of South and East  
58 Asia, as shown in Fig. S1 (Samset et al., 2019; Ramachandran et al., 2021).

59 Aerosols are the main pollutant of concern due to their adverse effects on  
60 atmospheric visibility and human health (Bell and Davis, 2001; Cohen et al., 2017).  
61 Besides their environmental impacts, aerosols can also influence the regional and global  
62 climate by changing the atmospheric radiation budget via scattering and absorbing solar  
63 radiation and modifying cloud microphysical properties (Yu et al., 2013; Yang et al.,  
64 2017a,b, 2019, 2020, 2022).

65 The East Asian summer monsoon (EASM) is a crucial component of the Asian  
66 atmospheric circulation and climate system, driven by the temperature difference  
67 between the Asian continent and its surrounding oceans (Ding and Chan, 2005). EASM  
68 provides 40–50% of the annual total precipitation for southern China, and 60–70% for  
69 northern China (Lei et al., 2011). Changes in EASM can have a significant impact on  
70 local infrastructure, agriculture, water resources and global water cycle (Ding and Chan,  
71 2005).

72 Many previous studies have illustrated the important role that AA has played in  
73 changing EASM (Lau et al., 2008; Li et al., 2016). Zhang et al. (2011) used the  
74 atmospheric general circulation model of the Beijing Climate Center (BCC\_AGCM)  
75 with prescribed sea surface temperature (SST) and sea ice concentration (SIC) to study  
76 the response of EASM to the direct radiative effects of AA. They reported that increases

77 in aerosols would cause anomalous northerlies, reduce the northward moisture transport,  
78 and weaken the EASM precipitation in eastern and southern China between 15°N and  
79 30°N. Using the National Center for Atmospheric Research (NCAR) Community  
80 Atmospheric Model version 5 (CAM5) driven by prescribed SST and SIC with aerosol  
81 direct, semi-direct and indirect effects considered, Jiang et al. (2013) investigated the  
82 AA impact on the EASM between 1850 and 2000. They concluded that the increased  
83 AA reduced the land-sea thermal contrast, reduced precipitation in North China, and  
84 increased precipitation in South China and its adjacent oceans, primarily attributed to  
85 the effects of sulfate and primary organic matter (POM) aerosols. Xie et al (2016) also  
86 indicated that the effects of AA on the monsoonal circulation and precipitation were  
87 stronger in weak monsoon years than in strong monsoon years based on CAM5  
88 simulations. Using a coupled atmosphere-ocean-mixed-layer model, Tian et al. (2018)  
89 and Dong et al. (2019) found that the increase in AA led to anomalous moisture flux  
90 divergence and decreased precipitation over northern China, which weakened the  
91 EASM during the recent decades. Mu and Wang (2020) used simulations from 16  
92 Coupled Model Intercomparison Project Phase 5 (CMIP5) models to quantitatively  
93 distinguish the fast (direct effects of forcing on radiation, cloud, and land surface  
94 processes excluding the ocean response) and slow (oceanic processes) responses of the  
95 EASM to aerosol forcing. They suggested that an increased AA can weaken the EASM  
96 circulation and reduce precipitation over eastern China and the main reason for this was  
97 the fast response of atmospheric processes to AA forcing.

98 Remote aerosol also can affect the circulation and precipitation of EASM. Cowan  
99 and Cai (2011) used a coupled climate model to study the effects of Asian and non-  
100 Asian AA on the EASM in the 20th century and indicated that non-Asian AA  
101 exacerbated the cooling over Europe and Asia relative to the surrounding oceans, and  
102 weakened the southerly wind, which suppresses the Asian summer monsoon  
103 precipitation. Wan et al. (2013) reported that, based on climate model simulations with  
104 prescribed SST, European black carbon (BC) aerosol enhanced tropospheric heating  
105 over the Eurasian Continent through a propagating wave train and horizontal air

106 temperature advection, which can intensify the land-sea thermal contrast and therefore  
107 enhance the EASM. Mahmood and Li (2014) also suggested that the South Asian BC  
108 aerosol could decrease EASM precipitation in China through weakening the moist air  
109 transport toward East Asia from the Bay of Bengal and enhancing atmospheric stability  
110 in the Yangtze River Basin. Based on the atmospheric component of the UK Met Office  
111 Hadley Centre Earth system model (HadGEM2-ES), Dong et al. (2015) found that  
112 anthropogenic sulfate from European emissions induced cooling and drying of the mid-  
113 troposphere over Asia and reduced the land-sea thermal contrast, which led to high sea  
114 level pressure (SLP) anomalies over Asia and low SLP anomalies over the Western  
115 North Pacific (WNP) and further weakened the EASM.

116 The previous studies that examined the effects of local and remote aerosols on the  
117 EASM have made a great contribution to our understanding of the response of East  
118 Asian climate to aerosols. The majority of model studies have suggested that the  
119 increase in AA over East Asia could weaken the EASM strength. However, few studies  
120 have explored the impacts of recent dipole changes in emissions of anthropogenic  
121 aerosols and their precursors over East Asia and South Asia on the EASM. In this study,  
122 we investigate the relative impacts of the decrease in AA emissions over East Asia and  
123 the increase in AA over South Asia between 2013 and 2017, based on the atmosphere  
124 model of the Community Earth System Model Version 2 (CESM2). The remainder of  
125 the paper is organized as follows. Section 2 describes the CESM2 model and  
126 experiments design. Section 3 analyzes the responses of EASM to the changing AA  
127 emissions from East and South Asia. Conclusions and discussions are given in Section  
128 4.

129

## 130 **2. Model description and experiment design**

131 In this study, the responses of EASM to AA emissions are examined using the  
132 Community Atmosphere Model version 6 (CAM6), which is the atmospheric  
133 component of CESM2 (Danabasoglu et al., 2020). Simulations are performed at a  
134 spatial resolution of  $0.9^\circ$  latitude  $\times$   $1.25^\circ$  longitude and 32 vertical layers from the

135 surface to 3.6 hPa. In CAM6, aerosols are treated using the 4-mode Modal Aerosol  
136 Model (X. Liu et al., 2016), which predicts the mass and number concentrations of  
137 major aerosol species including sulfate, BC, POM, SOA (secondary organic aerosol),  
138 mineral dust, and sea salt. Aerosols can interact with radiation, clouds and precipitation  
139 that are realistically represented in CAM6. Details of the CAM6/CESM2 can be found  
140 in Danabasoglu et al. (2020).

141 In this study, we use the CEDS (Community Emissions Data System)  
142 anthropogenic emissions of aerosols and precursors (Hoesly et al., 2018) that were  
143 developed for the CMIP6 (Coupled Model Intercomparison Project Phase 6) as the  
144 model input datasets. The anthropogenic emissions in China are replaced by Multi-  
145 resolution Emission Inventory for China (MEIC) inventory, which has been shown to  
146 produce the consistent aerosol precursor loadings with satellite observations (F. Liu et  
147 al., 2016) and better capture the recent emission reductions in China (Wang et al., 2021).  
148 Biomass burning emissions are also from the standard CMIP6 datasets (van Marle et  
149 al., 2017).

150 Three 40-year parallel equilibrium experiments, named BASE, EA17 and  
151 EASA17, are conducted with different AA emissions from East Asia and South Asia.  
152 The boundaries of East Asia and South Asia follow the source-receptor regions  
153 provided by the Hemispheric Transport of Air Pollution model experiment phase 2  
154 (HTAP2). The AA emissions in both East Asia and South Asia are fixed at year 2013  
155 levels in the BASE experiment, while East Asian emissions are changed to year 2017  
156 levels in EA17 and AA emissions in 2017 are adopted for both East Asia and South  
157 Asia in EASA17. AA emissions in other regions of the world remain at year 2013 levels  
158 in all simulations. The seasonal cycle of emissions is considered in the simulations. The  
159 differences between the BASE experiment and other two experiments (EA17 and  
160 EASA17) are attributed to the effect of AA emissions reduction in East Asia and the  
161 dipole changes in the AA emissions over East Asia and South Asia, respectively. All  
162 experiments are driven by the climatological mean SST and SIC for the present-day  
163 climatology (average over 1995–2005). We note that only atmospheric rapid

164 adjustments are considered in this study without the consideration of SST responses,  
165 and the land surface temperatures are allowed to respond to aerosol changes. The ozone,  
166 greenhouse gas forcing and biomass burning emissions are kept at year 2013 values  
167 during simulations. Each experiment runs for 40 years and the averages of the last 35  
168 years are used for analysis. Considering the uncertainty of the aerosol impacts on  
169 climate, the two-tailed Student's t test with 90% confidence level is applied in the  
170 following analysis.

171 Effective radiative forcing (ERF) quantifies the net change in the energy budget  
172 of the Earth system after a perturbation, and includes the instantaneous forcing and  
173 rapid adjustments from the atmosphere and surface (Smith et al., 2020). The ERF in  
174 this study is diagnosed as the difference of net radiative flux between the perturbation  
175 experiments (EA17 and EASA17) and the control experiment (BASE). ERF due to  
176 aerosol-cloud interactions is decomposed based on Ghan (2013), defined as  $\Delta(F_{clean} -$   
177  $F_{clear, clean})$ .  $F_{clean}$  is the radiative flux neglecting the scattering and absorption of solar  
178 radiation by aerosols and  $F_{clear, clean}$  is the radiative flux neglecting scattering and  
179 absorption by both clouds and aerosols. The difference between two simulations is  
180 represented by  $\Delta$ .

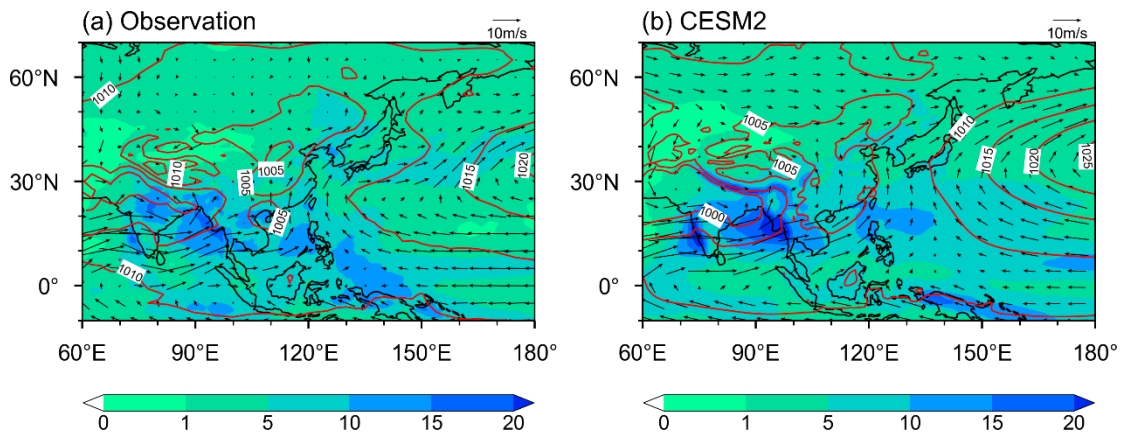
181

## 182 **3. Results**

### 183 **3.1. Model evaluation**

184 Observed atmospheric circulation and precipitation during the EASM season are  
185 shown in Fig. 1a, which are from the NCEP/NCAR Reanalysis (Kalnay et al., 1996),  
186 ERA5 Reanalysis (Hersbach et al., 2019) and Global Precipitation Climatology Project  
187 (GPCP) data sets (Adler et al., 2018). Generally, the monsoon flow carrying moist air  
188 from the Bay of Bengal and Indochina Peninsula penetrates abruptly into the Yangtze  
189 River Basin (26°–32°N, 105°–122.5°E) and extends to northern China (32°–42°N,  
190 105°–122.5°E). During this period, the western Pacific subtropical high (WPSH) over  
191 the east of China mainland is important for the atmospheric conditions and precipitation  
192 in China. CAM6 reproduces well the climatological mean of the main features of

193 EASM (Fig. 1b), although the precipitation in the Bay of Bengal and westerlies north  
 194 of 40°N are overestimated. The spatial correlation coefficients of boreal summer (JJA)  
 195 mean zonal and meridional winds at 850 hPa, SLP, and precipitation rate between  
 196 observation and BASE experiment in 2013 over Asian regions are 0.87, 0.83, 0.87, and  
 197 0.70, respectively, suggesting that CAM6 has the ability to simulate the key features of  
 198 EASM.  
 199



200  
 201 **Figure 1.** June-July-August (JJA) mean 850 hPa winds (vectors, m s<sup>-1</sup>), sea level  
 202 pressure (contours, hPa) and precipitation (shaded colors, mm day<sup>-1</sup>) in 2013 derived  
 203 from (a) NCEP/NCAR Reanalysis (for sea level pressure), ERA5 Reanalysis (for winds)  
 204 and Global Precipitation Climatology Project (GPCP) data set (for precipitation) and  
 205 (b) from the BASE experiment of CAM6.

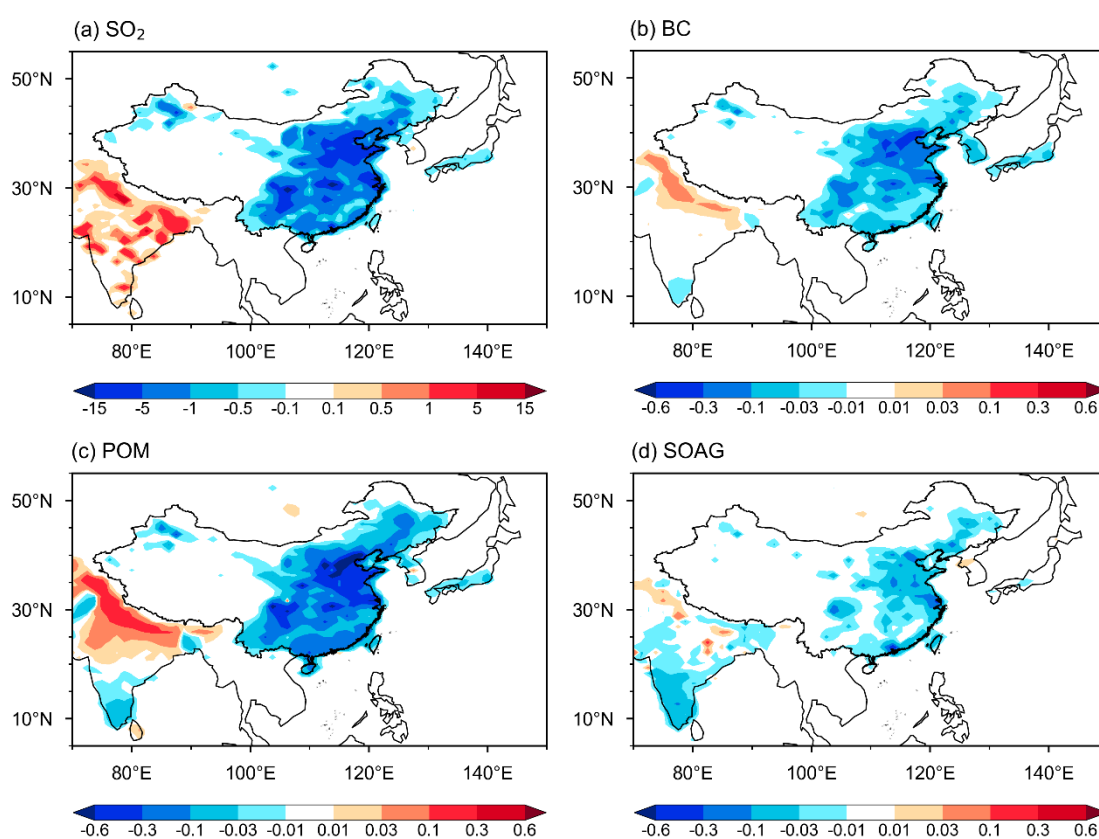
206  
 207 Changes in surface aerosol concentrations during 2013–2017 simulated by CAM6  
 208 were evaluated in Gao et al. (2022). It was reported that the model could capture the  
 209 changes in spatial distribution of aerosols concentrations in China, but strongly  
 210 underestimated the magnitude of the concentration decreases by more than 50%. The  
 211 low bias of the aerosol reduction could result in the underestimation of the responses in  
 212 EASM, which is further discussed in the following section.

### 213 3.2. Dipole changes in aerosol emissions, burden and effective radiative forcing

214 The changes in JJA mean anthropogenic emissions of BC, POM, sulfur dioxide  
 215 (SO<sub>2</sub>) and SOA precursor gas (SOAG) between 2013 and 2017 are shown in Fig. 2

216 (changes over East Asia or South Asia are given in Fig. S1). Anthropogenic emissions  
 217 of aerosols and precursor gases significantly decreased over eastern China from 2013  
 218 to 2017 due to the Air Pollution Prevention and Control Action Plan, but increased in  
 219 the Indo-Gangetic Plain (IGP) region (25°–35°N, 70°–90°E), displaying a dipole  
 220 pattern between East Asia and South Asia. The anthropogenic emissions over South  
 221 India also decreased during 2013–2017, which led to changes in burden of aerosols and  
 222 could influence climate in Asia.

223



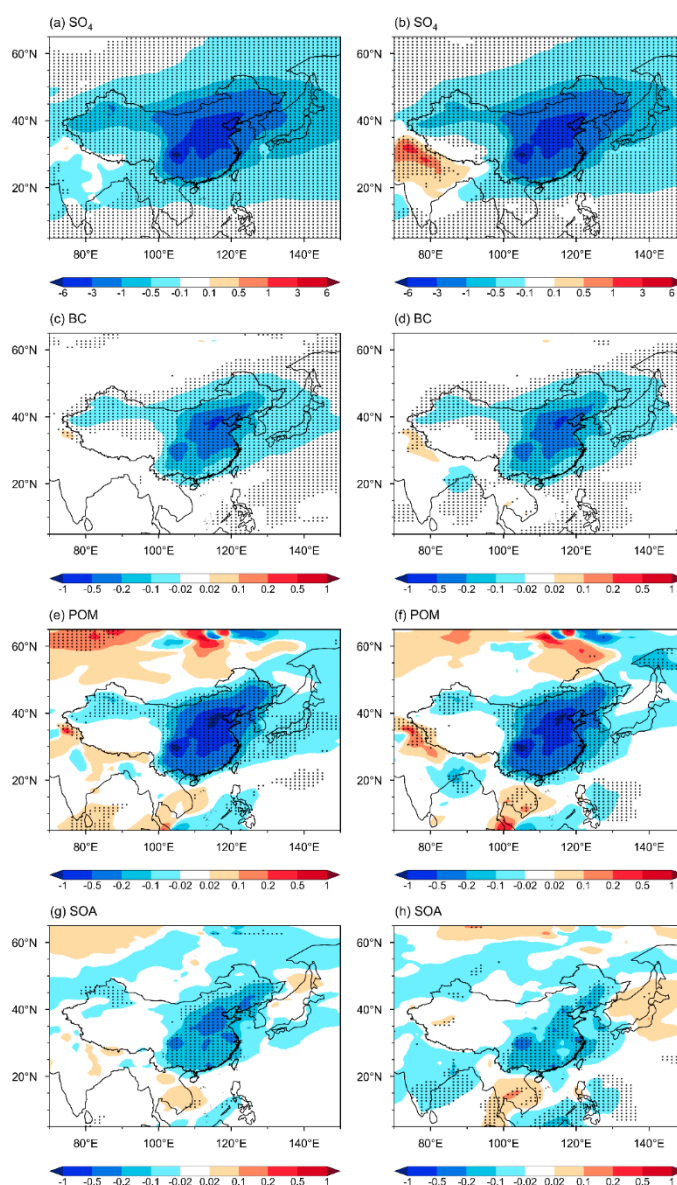
224

225 **Figure 2.** Changes in June-July-August (JJA) mean anthropogenic emissions of SO<sub>2</sub>,  
 226 BC, POM, and SOAG (g m<sup>-2</sup> year<sup>-1</sup>) between 2013 and 2017.

227

228 Changes in the spatial distribution of AA column burden are shown in Fig. 3 and  
 229 corresponding percentage changes are shown in Fig. S2. Due to the reduction in AA  
 230 emissions, the AA column burdens decreased significantly in East Asia in both EA17  
 231 and EASA17 experiments. Sulfate aerosol decreased most significantly, especially in

232 northern China by 3–6 mg m<sup>-2</sup> (40–60%), followed by POM (0.5–1 mg m<sup>-2</sup>, 10–30%),  
 233 BC (0.2–0.5 mg m<sup>-2</sup>, 20–40%), and SOA (0.2–0.5 mg m<sup>-2</sup>, 5–10%). In South Asia, the  
 234 changes in the column burden of AA between BASE and EASA17 are basically  
 235 consistent with the changes in anthropogenic emissions. The largest increases in AA  
 236 column burden are located over IGP regions. Relative to 2013, sulfate burden in 2017  
 237 was increased by 0.5–3 mg m<sup>-2</sup> (10–20%), followed by POM (0.1–0.5 mg m<sup>-2</sup>, 1–10%)  
 238 and BC (0.02–0.1 mg m<sup>-2</sup>, 1–10%), while SOA burden showed a weak decrease of less  
 239 than 5% over South Asia.  
 240



241

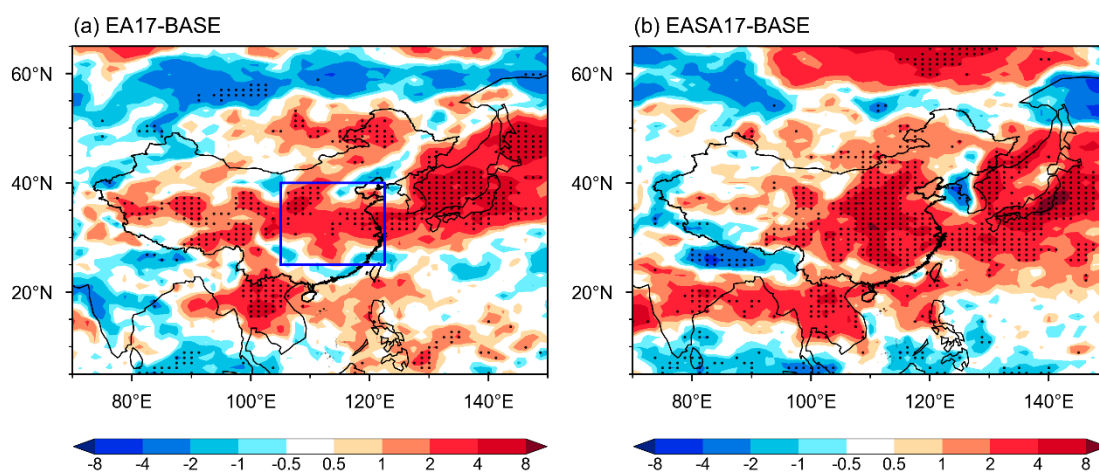
242 **Figure 3.** Changes in JJA mean column burden of (a, b) sulfate, (c, d) BC, (e, f) POM

243 and (g, h) and SOA ( $\text{mg m}^{-2}$ ) between BASE and EA17 (EA17–BASE) and between  
244 BASE and EASA17 (EASA17–BASE), respectively. The dotted areas indicate  
245 statistical significance with 90% confidence based on a two-tailed Student's t test.

246

247 As shown in Fig. 4a, the decrease in AA led to the positive aerosol ERF at the top  
248 of the atmosphere (TOA) over central-eastern China between 2013 and 2017, with a  
249 maximum change of  $4\text{--}8 \text{ W m}^{-2}$ . Averaged over central-eastern China ( $25^{\circ}\text{--}40^{\circ}\text{N}$ ,  
250  $105^{\circ}\text{--}122.5^{\circ}$ ), 2013-to-2017 changes in AA emissions induced a positive aerosol ERF  
251 of  $1.59 (\pm 0.97) \text{ W m}^{-2}$  (Table 1) relative to BASE. The decreases in AA emissions from  
252 East Asia also resulted in strong positive ERF of  $2\text{--}8 \text{ W m}^{-2}$  over Japan and the  
253 surrounding ocean. The changes in ERF are primarily due to aerosol-cloud interactions  
254 in the case of AA emission reductions (Fig. S3). The decreases in aerosols transported  
255 to the western north Pacific caused the weakened negative ERF due to aerosol-cloud  
256 interactions, leading to an increase in radiation absorption by the Earth. In addition, the  
257 decrease in BC aerosols suppressed the formation of low-level marine stratocumulus  
258 and increased high-level cloud amount over the western north Pacific (Fig. S4), as  
259 previously reported by Yang et al. (2019), which further intensified the positive aerosol  
260 ERF in EA17 relative to BASE. The reduced AA emissions in East Asia also led to  
261 stronger positive ERF at the surface than at TOA over central-eastern China, revealing  
262 the weakened atmospheric absorption by absorbing aerosols related to the emission  
263 reductions (Fig. S5).

264



265

266 **Figure 4.** Changes in JJA mean aerosol ERF ( $\text{W m}^{-2}$ ) (a) between BASE and EA17  
 267 (EA17–BASE) and (b) between BASE and EASA17 (EASA17–BASE). The dotted  
 268 areas indicate statistical significance with 90% confidence based on a two-tailed  
 269 Student’s t test. The blue box in (a) marks central-eastern China ( $25^{\circ}$ – $40^{\circ}$ N,  
 270  $105^{\circ}$ – $122.5^{\circ}$ E).

271

272 **Table 1** Regional mean differences in effective radiative forcing (ERF), temperature at  
 273 2 meter (T2m), meridional wind at 850 hPa (V850) and precipitation rate between  
 274 EA17 and BASE and between EA17 and EASA17 over central-eastern China ( $25^{\circ}$ –  
 275  $40^{\circ}$ N,  $105^{\circ}$ – $122.5^{\circ}$ E) in JJA.  $1\sigma$  for the 35 seasonal means is shown in the parentheses.

276

Experiment	ERF ( $\text{W m}^{-2}$ )	T2m ( $^{\circ}\text{C}$ )	V850 ( $\text{m s}^{-1}$ )	Precipitation ( $\text{mm day}^{-1}$ )
EA17-BASE	+1.59 ( $\pm 0.97$ )	+0.09 ( $\pm 0.07$ )	+0.25 ( $\pm 0.22$ )	+0.32 ( $\pm 0.16$ )
EASA17-BASE	+3.39 ( $\pm 0.89$ )	+0.20 ( $\pm 0.08$ )	+0.39 ( $\pm 0.21$ )	–0.07 ( $\pm 0.16$ )

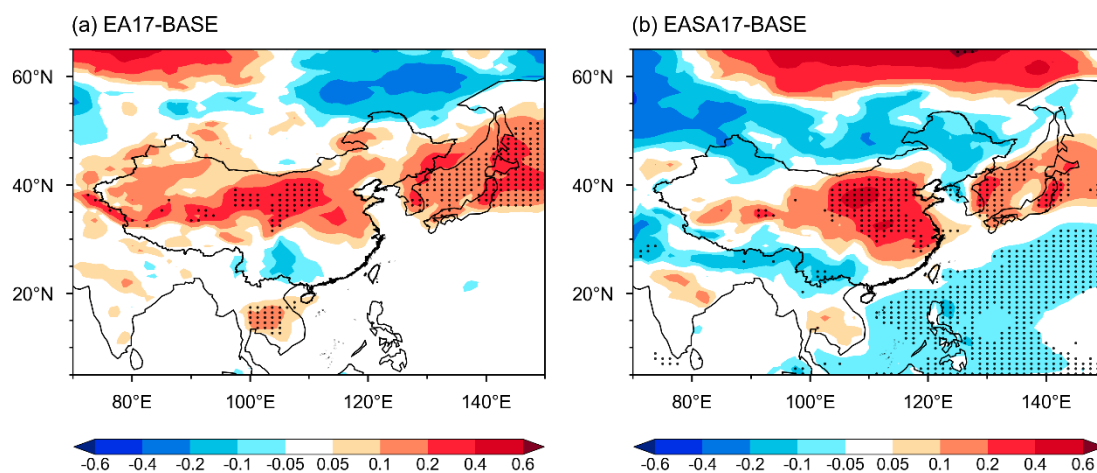
277

278 Due to the increases in AA emissions over the IGP region, the negative ERF of  
 279 AA was strengthened by  $2$ – $8 \text{ W m}^{-2}$  during 2013–2017, while positive ERF was located  
 280 over South India (Fig. 4b) due to the decrease in low-level cloud (Fig. S4b) during this  
 281 time period. Interestingly, the positive ERF over eastern China due to the decreases in  
 282 AA emissions over East Asia was strengthened by the increases in emissions over South  
 283 Asia. The regional averaged ERF over central-eastern China increased from  $1.59 (\pm 0.97)$   
 284  $\text{W m}^{-2}$  in EA17 to  $3.39 (\pm 0.89) \text{ W m}^{-2}$  in EASA17, relative to BASE experiment, likely  
 285 due to feedbacks through changes in atmospheric circulation and clouds associated with  
 286 the increases in AA emissions from South Asia, which is further examined below.

### 287 3.3. Change in East Asian climate due to the dipole changes in emissions

288 The perturbation of radiation flux associated with the dipole changes in AA  
 289 emissions during 2013–2017 can further change the surface air temperature, as shown  
 290 in Fig. 5. Due to the reductions in AA emissions from East Asia, surface air temperature  
 291 increased between  $30^{\circ}$ N and  $45^{\circ}$ N over China and the downwind western north Pacific,

292 with the maximum temperature increase of 0.2–0.4 °C (Fig. 5a). Temperature also  
 293 decreased in southwestern China and increased in Southeast Asia, likely resulting from  
 294 the increase/decrease in mid-level cloud (Fig. S4c) caused by the aerosol-induced  
 295 changes in atmospheric circulation. When considering both the decrease in AA  
 296 emissions in East Asia and the increase in AA emissions in South Asia, surface  
 297 temperature shows a weak decrease over the IGP region, but the temperature increase  
 298 in central-eastern China was stronger, with the maximum temperature increase of 0.4–  
 299 0.6 °C (Fig. 5b). A weak cooling appears over the northwestern Pacific, which may be  
 300 related to the downdraft of cold air due to the strengthened WPSH (Yang et al., 2022).  
 301 Averaged over central-eastern China, the surface air temperature anomaly induced by  
 302 the reductions in AA emissions from East Asia was doubled, from 0.09 ( $\pm 0.07$ ) °C to  
 303 0.20 ( $\pm 0.08$ ) °C (Table 1), with the simultaneous increase in AA emissions from South  
 304 Asia.  
 305

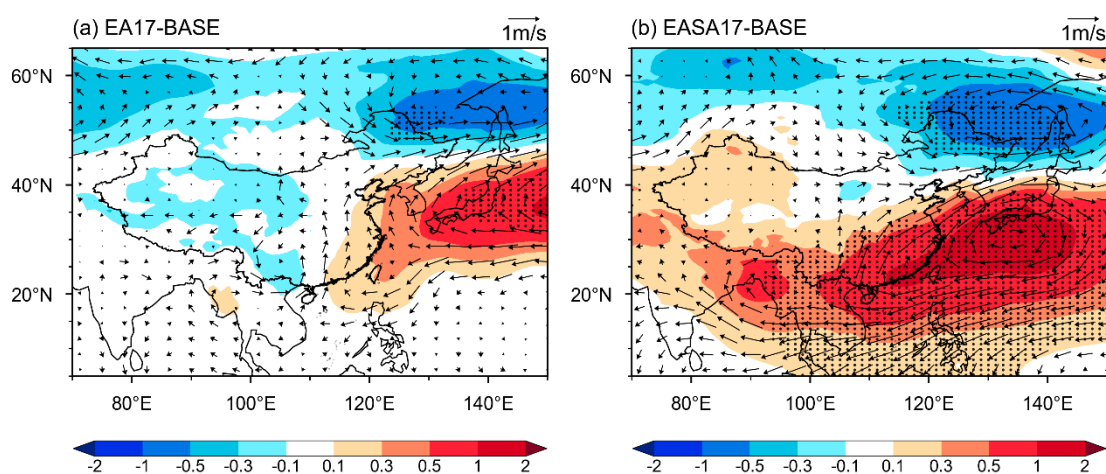


306  
 307 **Figure 5.** Changes in JJA mean surface air temperature (°C) (a) between BASE and  
 308 EA17 (EA17–BASE) and (b) between BASE and EASA17 (EASA17–BASE). The  
 309 dotted areas indicate statistical significance with 90% confidence based on a two-tailed  
 310 Student's t test.

311  
 312 The enhanced summer warming over central-eastern China in EASA17, compared  
 313 to EA17, is the result of the intensified and westward shift of the WPSH that can be

314 linked to the increase in BC aerosol in South Asia. The enhanced warming over land  
 315 caused by the reductions in East Asian emissions of AA intensified the land-sea thermal  
 316 contrast between eastern China and the western north Pacific, resulting in a  
 317 strengthened WPSH (Fig. 6a). The increases in BC aerosols in South Asia led to  
 318 anomalous atmospheric heating over 70–80°E (Fig. S6a), which produced an  
 319 anomalous ascending flow over this region (Fig. S6b). The anomalous ascend over  
 320 South Asia enhanced the anomalous subsidence over 110–130°E, causing the  
 321 intensified and westward shift of the WPSH (Fig. S7a), adding to the effect of  
 322 reductions in AA emissions from East Asia (Fig. 6b). The enhanced intensity and  
 323 westward shift of WPSH can increase the atmospheric stability and suppress the cloud  
 324 formation (Fig. S4), leading to a warmer climate over central-eastern China in EASA17  
 325 than in EA17.

326



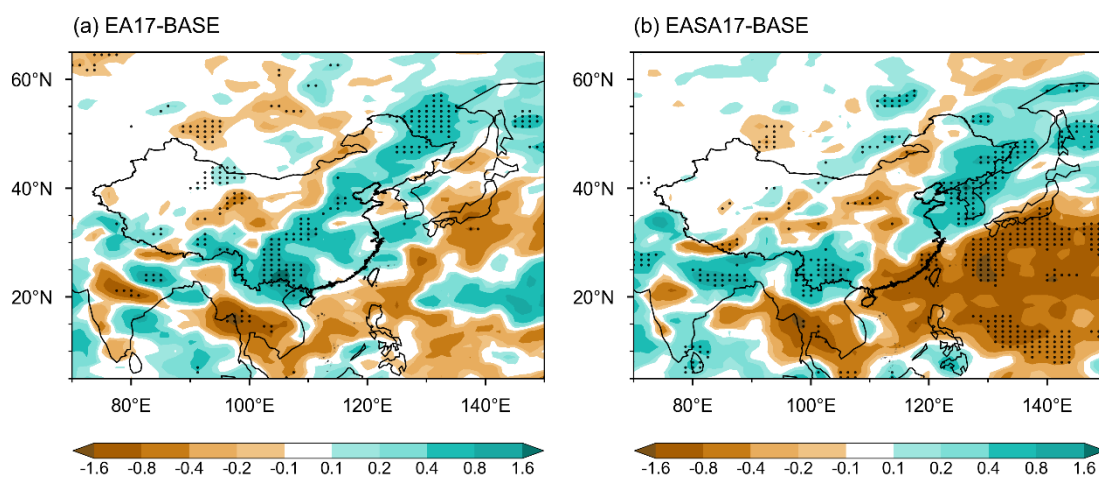
327

328 **Figure 6.** Changes in JJA mean sea level pressure (colors, hPa) and 850 hPa winds  
 329 (vectors,  $\text{m s}^{-1}$ ) (a) between BASE and EA17 (EA17–BASE) and (b) between BASE  
 330 and EASA17 (EASA17–BASE). The dotted areas indicate statistical significance with  
 331 90% confidence based on a two-tailed Student's t test.

332

333 The most significant feature of precipitation changes due to the reductions in AA  
 334 emissions from East Asia was an enhanced summer rainfall over central-eastern China  
 335 (Fig. 7a). It was related to the anomalous southerly winds along the west edge of the  
 336 strengthened WPSH (Fig. 6a), which brought warm and moist air from South China

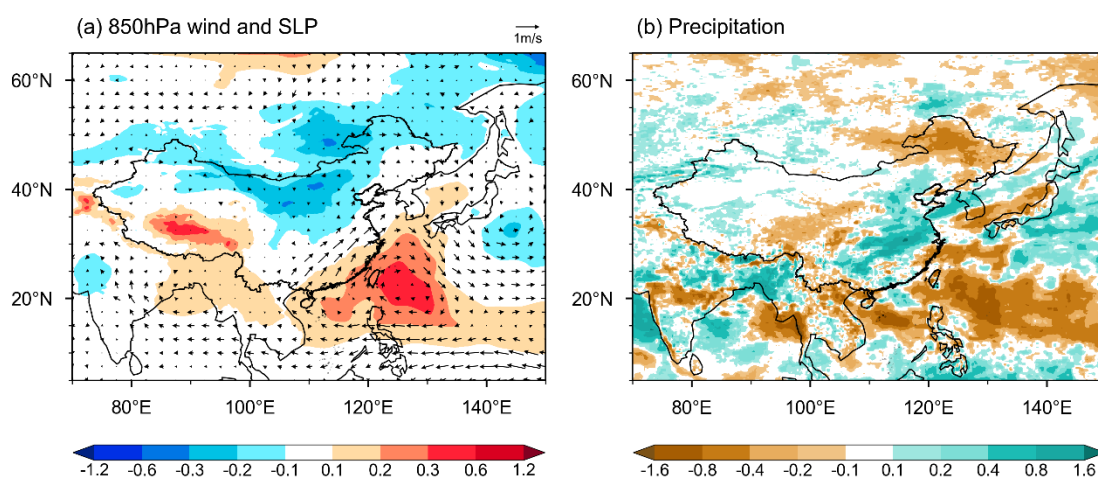
337 Sea to southern China ( $18^{\circ}$ – $32^{\circ}$ N,  $105^{\circ}$ – $122.5^{\circ}$ E), and increased cloud amount there  
 338 (Figs. S4a, S4c and S4e). Averaged over central-eastern China, the JJA precipitation  
 339 was increased by  $0.32 (\pm 0.16)$  mm day<sup>-1</sup> in EA17 compared to BASE experiment (Table  
 340 1). The impact of the dipole pattern of the Asian AA emission changes on EASM  
 341 precipitation is complex (Fig. 7b). Although precipitation in central-eastern China  
 342 increased due to the anomalous moisture transport associated with the East Asian  
 343 emission reductions, the westward shift of WPSH due to the South Asian emission (Fig.  
 344 S7a) increased the atmospheric stability and tended to decrease precipitation over  
 345 central eastern China and the western north Pacific (Fig. S7b). This can be further  
 346 confirmed by the anomalous downdraft over  $20^{\circ}$ – $40^{\circ}$ N in central-eastern China (Fig.  
 347 S8b). The dipole changes in emissions caused increased precipitation in the northeast  
 348 (the Korean peninsula) and southwest (Yunnan/Myanmar border), but deficits in the  
 349 central and southeast regions, with an insignificant regional averaged change of  $-0.07$   
 350 ( $\pm 0.16$ ) mm day<sup>-1</sup> in EASA17 compared to BASE experiment.  
 351



352  
 353 **Figure 7.** Changes in JJA mean precipitation (mm day<sup>-1</sup>) (a) between BASE and EA17  
 354 (EA17–BASE) and (b) between BASE and EASA17 (EASA17–BASE). The dotted  
 355 areas indicate statistical significance with 90 % confidence based on a two-tailed  
 356 Student's t test.  
 357

358 The changes in JJA mean SLP, 850hPa winds and precipitation between 2013  
 359 (average of 2011–2015 to remove the internal variability in observations) and 2017  
 360 (average of 2015–2019) from observations are also shown in Fig. 8 and Fig. S9 for

361 reference. During 2013–2017, observations also show the intensified and westward  
 362 shift of WPSH and the increases in the southwesterly winds over southern China,  
 363 similar to the modeling results, indicating that the recent change in EASM circulation  
 364 can be largely explained by the dipole changes in AA emissions over East Asia and  
 365 South Asia. The observed EASM precipitation increased over central-eastern China and  
 366 decreased over the western north Pacific in 2017 compared to 2013, similar to the  
 367 effects of East Asian emission changes in model. Note that, however, the changes in  
 368 atmospheric circulation and precipitation of EASM are affected by many other factors  
 369 than aerosols, such as climate change, changes in SST, and modes of internal variability.  
 370 A few differences are also shown in observations, such as the increase in precipitation  
 371 over central China and the less significant enhancement of WPSH in observations,  
 372 which can not be explained by the changes in AA alone. In addition, the model  
 373 underestimated the aerosol decrease in eastern China during 2013–2017 (Gao et al.,  
 374 2022), which can lead to a low bias in the simulated response of EASM precipitation  
 375 to AA emission reductions from East Asia.  
 376



377  
 378 **Figure 8.** Changes in JJA mean (a) sea level pressure (colors, hPa) and 850hPa winds  
 379 (vectors,  $\text{m s}^{-1}$ ), and (b) precipitation rate ( $\text{mm day}^{-1}$ ) between 2013 (represented by the  
 380 average of 2011–2015) and 2017 (represented by the average of 2015–2019) derived  
 381 from ERA5.  
 382

### 383 **3.4. Quantifying the change in EASM intensity**

384 As examined above, the decreases in AA emissions from East Asia intensified  
385 WPSH and the increases in AA emissions from South Asia further led to the westward  
386 shift of WPSH, enhancing the intensity of EASM (Wang et al., 2013). However, to what  
387 extent the dipole changes in AA emissions over East Asia and South Asia influence the  
388 EASM needs quantitative analysis.

389 In this study, three indices (i.e.,  $I_{Sun}$ ,  $I_{Lau}$  and  $I_{Wu}$ ) that include different features of  
390 east-west and north-south thermal contrast (Sun et al., 2002), north-south shear vorticity  
391 (Lau et al., 2000) and southwest monsoon (Wu et al., 1997), respectively, are employed  
392 to quantify the intensity of EASM, as shown in Table S1. The three indices are  
393 individually calculated using surface air temperature, zonal winds at 200 hPa and  
394 meridional winds at 850 hPa, respectively. Using three different indices can give a more  
395 robust result than that from any individual index.

396 Compared to the BASE experiment, the EASM intensity in EA17 is increased by  
397 4.1%, 0.6%, and 4.5%, respectively, for  $I_{Sun}$ ,  $I_{Lau}$ , and  $I_{Wu}$ , indicating that the reductions  
398 in AA emissions from East Asia during 2013–2017 enhanced the EASM strength by  
399 less than 5%. With the effects of increases in AA emissions from South Asia  
400 superimposed, the increases are enlarged to 14.9%, 9.4%, and 5.0% in the EASA17  
401 experiment. It suggests that, besides the decreases in East Asian emissions, the  
402 increases in South Asian emissions of AA have a crucial impact on the intensified  
403 EASM strength. The dipole changes in AA emissions over East Asia and South Asia  
404 together enhanced the EASM by 5–15% during 2013–2017.

405

### 406 **4. Conclusions and discussion**

407 China implemented the air pollution prevention and control action plan in 2013,  
408 which significantly reduced the emissions of anthropogenic aerosols (AA) and  
409 precursors. Meanwhile, AA emissions in South Asia have been continually increasing,  
410 which formed a dipole pattern of changes in AA emissions between South Asia and East  
411 Asia during 2013–2017. In this study, the response of EASM to the dipole changes in

412 AA emissions are investigated based on CESM2-CAM6 emissions sensitivity  
413 simulations.

414 Along with the decreases in East Asian AA emissions, a positive aerosol ERF of  
415  $1.59 (\pm 0.97) \text{ W m}^{-2}$  relative to BASE appears in central-eastern China ( $25^{\circ}$ – $40^{\circ}\text{N}$ ,  
416  $105^{\circ}$ – $122.5^{\circ}\text{E}$ ) in summer, resulting in a  $0.09 (\pm 0.07) ^{\circ}\text{C}$  warming during 2013–2017.  
417 The anomalous warming over land intensified the land-sea thermal contrast between  
418 eastern China and the western north Pacific, which resulted in a strengthened WPSH  
419 and an increase in summer precipitation by  $0.32 (\pm 0.16) \text{ mm day}^{-1}$  over central-eastern  
420 China. When considering both the AA reductions in East Asia and increases in South  
421 Asia, the ERF relative to BASE is increased to  $3.39 (\pm 0.89) \text{ W m}^{-2}$ , along with an  
422 enhanced warming of  $0.20 (\pm 0.08) ^{\circ}\text{C}$  over central-eastern China, which is the result of  
423 westward shift of the strengthened WPSH linked to the increase in BC aerosol in South  
424 Asia. The combined effect of the stabilized air and moisture transport associated with  
425 the WPSH led to a  $-0.07 (\pm 0.16) \text{ mm day}^{-1}$  precipitation change related to the changes  
426 in Asian AA emissions during 2013–2017.

427 Based on the quantitative estimation of multiple EASM indices, the reductions in  
428 AA emissions from East Asia during 2013–2017 are found to enhance the EASM  
429 strength by less than 5%, while the dipole changes in AA emissions over East Asia and  
430 South Asia together enhanced the EASM by 5–15% during 2013–2017, revealing an  
431 important role of South Asian AA emissions in changing the East Asian climate.  
432 However, we also note that although the dipole pattern of changes in AA emissions over  
433 Asia leads to stronger land-sea thermal contrast and circulations changes in comparison  
434 with responses to AA reductions over East Asia alone, precipitation does not show a  
435 stronger response to the dipole changes in AA emissions over East Asia and South Asia  
436 due to precipitation suppression caused by South Asian AA emissions.

437 This study focuses on the EASM response to Asian emissions dipole changes in  
438 JJA. However, change in AA in pre- and post- monsoon seasons may also influence the  
439 climate in East Asia (Ramachandran et al., 2020). As shown in Fig. S10, the responses  
440 of circulation and precipitation over central-eastern China to changes in East Asian AA

441 emissions reach their maximums in JJA, while temperature response decreases from  
442 April to September. With both changes in AA emissions over East Asia and South Asia  
443 included, the climate responses are strongest in July, while the South Asian emissions  
444 enhance precipitation in September.

445 Note that, Gao et al. (2022) used the same model to investigate the climatic  
446 impacts of changes in aerosols and ozone due to China's recent clean air actions by  
447 perturbing aerosol emissions and ozone concentrations over China. They found that the  
448 increase in ozone can intensify the warming caused by the aerosol reductions in China.  
449 Our study answers how and to what extent the spatial dipole pattern in Asian aerosol  
450 changes could influence EASM through changing AA emissions over East Asia and  
451 South Asia, which has the different scientific focus and experimental design compared  
452 to Gao et al. (2022).

453 Our study also has some limitations and uncertainties. Firstly, although the  
454 atmospheric rapid adjustments were previously reported as the main process of EASM  
455 response to AA (Mu and Wang, 2020), the dipole pattern of AA emissions can also  
456 influence the EASM through slow oceanic processes and air-sea interactions, which  
457 deserves further investigation by performing simulations with the consideration of SST  
458 responses. Secondly, the current version of CESM2-CAM6 does not treat nitrate and  
459 ammonium aerosols; however, their changes in 2013–2017 could also affect the EASM,  
460 although slight changes were found in nitrate concentration in Beijing during this time  
461 (Zhang et al., 2020). Third, the model strongly underestimates the magnitude of  
462 regional surface aerosol concentrations (Gao et al., 2022; Ren et al., 2021; Yang et al.,  
463 2017a, c) and, therefore, the reduction in AA burden in China is also likely to be  
464 underestimated, which may lead to a low bias of the response of EASM to the changes  
465 in AA emissions from East Asia. Last but not the least, the conclusions here are based  
466 on the CESM2-CAM6 simulations, and therefore more comprehensive study is  
467 required in the future to conclusively answer the question as to what extent the dipole  
468 influences the EASM.

469 **Acknowledgments**

470 This study was supported by the National Natural Science Foundation of China (grant  
471 41975159), the National Key Research and Development Program of China (grant  
472 2019YFA0606800 and 2020YFA0607803), Jiangsu Science Fund for Distinguished  
473 Young Scholars (grant BK20211541) and Jiangsu Science Fund for Carbon Neutrality  
474 (grant BK20220031). H.W. acknowledges support from the U.S. Department of Energy  
475 (DOE), Office of Science, Office of Biological and Environmental Research (BER), as  
476 part of the Earth and Environmental System Modeling program. The Pacific Northwest  
477 National Laboratory (PNNL) is operated for DOE by the Battelle Memorial Institute  
478 under contract DE-AC05-76RLO1830.

479

480

481 **Data availability**

482 Observed sea level pressure in section 3.1 is available at  
483 <https://psl.noaa.gov/data/gridded/data.ncep.reanalysis.html> (last access: October 2022).  
484 Observed 850 hPa winds in section 3.1 and 3.3 are available at  
485 [https://cds.climate.copernicus.eu/cdsapp#!/dataset/reanalysis-era5-pressure-levels-  
486 monthly-means?tab=form](https://cds.climate.copernicus.eu/cdsapp#!/dataset/reanalysis-era5-pressure-levels-monthly-means?tab=form) (last access: October 2022). Observed precipitation rate in  
487 section 3.1 is available at [https://www.ncei.noaa.gov/data/global-precipitation-  
488 climatology-project-gpcp-daily/access/2013](https://www.ncei.noaa.gov/data/global-precipitation-climatology-project-gpcp-daily/access/2013) (last access: October 2022). Observed sea  
489 level pressure and precipitation rate in section 3.3 are available at  
490 [https://cds.climate.copernicus.eu/cdsapp#!/dataset/reanalysis-era5-single-levels-  
491 monthly-means?tab=form](https://cds.climate.copernicus.eu/cdsapp#!/dataset/reanalysis-era5-single-levels-monthly-means?tab=form) (last access: October 2022). The CESM2 model is available  
492 at [https://escomp.github.io/CESM/versions/cesm2.1/html/downloading\\_cesm.html](https://escomp.github.io/CESM/versions/cesm2.1/html/downloading_cesm.html)  
493 (last access: October 2022). The MEIC inventory can be downloaded at  
494 [http://meicmodel.org/?page\\_id=541&lang=en](http://meicmodel.org/?page_id=541&lang=en) (last access: October 2022).

495

496

497 **References**

- 498 Adler, R. F., Sapiano, M., Huffman, G. J., Wang, J. -J., Gu, G., Bolvin, D., Chiu, L.,  
499 Schneider, U., Becker, A., Nelkin, E., Xie, P., Ferraro, R., and Shin D, -B.: The  
500 Global Precipitation Climatology Project (GPCP) Monthly Analysis (New Version  
501 2.3) and a Review of 2017 Global Precipitation, *Atmosphere*, 9, 138,  
502 <https://doi.org/10.3390/atmos9040138>, 2018.
- 503 Bell, M. L., and Davis, D. L.: Reassessment of the lethal London fog of 1952: novel  
504 indicators of acute and chronic consequences of acute exposure to air pollution,  
505 *Environ. Health Perspect*, 109, 389–394, <https://doi.org/10.1289/ehp.01109s33389>,  
506 2001.
- 507 Cohen, A. J., Brauer, M., Burnett, R., Anderson, H. R., Frostad, J., Estep, K.,  
508 Balakrishnan, K., Brunekreef, B., Dandona, L., Dandona, R., Feigin, V., Freedman,  
509 G., Hubbell, B., Jobling, A., Kan, H., Knibbs, L., Liu, Y., Martin, R., Morawska, L.,  
510 Pope, C. A., 3rd, Shin, H., Straif, K., Caddick, G., Thomas, M., van Dingenen, R.,  
511 van Donkelaar, A., Vos, T., Murray, C. J. L., and Forouzanfar, M. H.: Estimates and  
512 25-year trends of the global burden of disease attributable to ambient air pollution:  
513 an analysis of data from the Global Burden of Diseases Study 2015, *The Lancet*,  
514 389, 1907–1918, [https://doi.org/10.1016/s0140-6736\(17\)30505-6](https://doi.org/10.1016/s0140-6736(17)30505-6), 2017.
- 515 Cowan, T., and Cai, W.: The impact of Asian and non-Asian anthropogenic aerosols on  
516 20th century Asian summer monsoon, *Geophys. Res. Lett.*, 38, L11703,  
517 <https://doi.org/10.1029/2011gl047268>, 2011.
- 518 Danabasoglu, G., Lamarque, J. -F., Bacmeister, J., Bailey, D. A., DuVivier, A. K.,  
519 Edwards, J., Emmons, L. K., Fasullo, J., Garcia, R., Gettelman, A., Hannay, C.,  
520 Holland, M. M., Large, W. G., Lauritzen, P. H., Lawrence, D. M., Lenaerts, J. T. M.,  
521 Lindsay, K., Lipscomb, W. H., Mills, M. J., Neale, R., Oleson, K. W., Otto Bliesner,  
522 B., Phillips, A. S., Sacks, W., Tilmes, S., Kampenhout, L., Vertenstein, M., Bertini,  
523 A., Dennis, J., Deser, C., Fischer, C., Fox Kemper, B., Kay, J. E., Kinnison, D.,  
524 Kushner, P. J., Larson, V. E., Long, M. C., Mickelson, S., Moore, J. K., Nienhouse,  
525 E., Polvani, L., Rasch, P. J., and Strand, W. G.: The Community Earth System  
526 Model Version 2 (CESM2), *J. Adv. Model Earth Sy.*, 12, e2019MS001916,  
527 <https://doi.org/10.1029/2019ms001916>, 2020.

528 Ding, Y. H., and Chan, J. C. L.: The East Asian summer monsoon: An overview,  
529 Meteorol. Atmos. Phys., 89, 117–142, <https://doi.org/10.1007/s00703-005-0125-z>,  
530 2005.

531 Dong, B., Sutton, R. T., Highwood, E. J., and Wilcox, L. J.: Preferred response of the  
532 East Asian summer monsoon to local and non-local anthropogenic sulphur dioxide  
533 emissions, *Clim. Dyn.*, 46, 1733–1751, [https://doi.org/10.1007/s00382-015-2671-](https://doi.org/10.1007/s00382-015-2671-5)  
534 5, 2015.

535 Dong, B., Wilcox, L. J., Highwood, E. J., and Sutton, R. T.: Impacts of recent decadal  
536 changes in Asian aerosols on the East Asian summer monsoon: roles of aerosol–  
537 radiation and aerosol–cloud interactions, *Clim. Dyn.*, 53, 3235–3256,  
538 <https://doi.org/10.1007/s00382-019-04698-0>, 2019.

539 Gao, J., Yang, Y., Wang, H., Wang, P., Li, H., Li, M., Ren, L., Yue, X., and Liao, H.:  
540 Fast climate responses to emission reductions in aerosol and ozone precursors in  
541 China during 2013–2017, *Atmos. Chem. Phys.*, 22, 7131–7142,  
542 <https://doi.org/10.5194/acp-22-7131-2022>, 2022.

543 Ghan, S. J.: Technical Note: Estimating aerosol effects on cloud radiative forcing,  
544 *Atmos. Chem. Phys.*, 13, 9971–9974, <https://doi.org/10.5194/acp-13-9971-2013>,  
545 2013.

546 Hersbach, H., Bell, B., Berrisford, P., Hirahara, S., Horányi, A., Muñoz Sabater, J.,  
547 Nicolas, J., Peubey, C., Radu, R., Schepers, D., Simmons, A., Soci, C., Abdalla, S.,  
548 Abellan, X., Balsamo, G., Bechtold, P., Biavati, G., Bidlot, J., Bonavita, M., Chiara,  
549 G., Dahlgren, P., Dee, D., Diamantakis, M., Dragani, R., Flemming, J., Forbes, R.,  
550 Fuentes, M., Geer, A., Haimberger, L., Healy, S., Hogan, R. J., Hólm, E., Janisková,  
551 M., Keeley, S., Laloyaux, P., Lopez, P., Lupu, C., Radnoti, G., Rosnay, P., Rozum,  
552 I., Vamborg, F., Sebastien, V., Thépaut, J.-N.: The ERA5 global reanalysis, *Q. J. R.*  
553 *Meteorol. Soc.*, 146, 1999–2049, <https://doi.org/10.1002/qj.3803>, 2020.

554 Hoesly, R. M., Smith, S. J., Feng, L., Klimont, Z., Janssens Maenhout, G., Pitkanen, T.,  
555 Seibert, J. J., Vu, L., Andres, R. J., Bolt, R. M., Bond, T. C., Dawidowski, L., Kholod,  
556 N., Kurokawa, J.-I., Li, M., Liu, L., Lu, Z., Moura, M. C. P., O’Rourke, P. R., and  
557 Zhang, Q.: Historical (1750–2014) anthropogenic emissions of reactive gases and  
558 aerosols from the Community Emissions Data System (CEDS), *Geosci. Model Dev.*,  
559 11, 369–408, <https://doi.org/10.5194/gmd-11-369-2018>, 2018.

560 Jiang, Y., Liu, X., Yang, X. -Q., and Wang, M.: A numerical study of the effect of  
561 different aerosol types on East Asian summer clouds and precipitation, *Atmos.*  
562 *Environ.*, 70, 51–63, <https://doi.org/10.1016/j.atmosenv.2012.12.039>, 2013.

563 Kalnay, E., Kanamitsu, M., Kistler, R., Collins, W., Deaven, D., Gandin, L., Iredell, M.,  
564 Saha, S., White, G., Woollen, J., Zhu, Y., Chelliah, M., Ebisuzaki, W., Higgins, W.,  
565 Janowiak, J., Mo, K. C., Ropelewski, C., Wang, J., Leetmaa, A., Reynolds, R.,  
566 Jenne, R., and Joseph, D: The NCEP/NCAR 40-Year Reanalysis Project, *B. AM.*  
567 *Meteorol. Soc.*, 77, 437–472, [https://doi.org/10.1175/1520-](https://doi.org/10.1175/1520-0477(1996)077<0437:TNYRP>2.0.CO;2)  
568 [0477\(1996\)077<0437:TNYRP>2.0.CO;2](https://doi.org/10.1175/1520-0477(1996)077<0437:TNYRP>2.0.CO;2), 1996.

569 Lau, K. -M., Ramanathan, V., Wu, G. -X., Li, Z., Tsay, S. C., Hsu, C., Sikka, R., Holben,  
570 B., Lu, D., Tartari, G., Chin, M., Koudelova, P., Chen, H., Ma, Y., Huang, J.,  
571 Taniguchi, K., and Zhang, R.: The Joint Aerosol–Monsoon Experiment: A New  
572 Challenge for Monsoon Climate Research, *B. Am. Meteorol. Soc.*, 89, 369–384,  
573 <https://doi.org/10.1175/bams-89-3-369>, 2008.

574 Lau, K. -M., Kim, K. -M., Yang, S.: Dynamical and boundary forcing characteristics of  
575 regional components of the Asia summer monsoon, *J. Climate.*, 13, 2461–2482,  
576 [https://doi.org/10.1175/1520-0442\(2000\)013<2461:DABFCO>2.0.CO;2](https://doi.org/10.1175/1520-0442(2000)013<2461:DABFCO>2.0.CO;2), 2000.

577 Lei, Y., Hoskins, B., and Slingo, J.: Exploring the Interplay between Natural Decadal  
578 Variability and Anthropogenic Climate Change in Summer Rainfall over China.  
579 Part I: Observational Evidence, *J. Climate.*, 24, 4584–4599,  
580 <https://doi.org/10.1175/2010jcli3794.1>, 2011.

581 Li, Z., Lau, W. K. -M., Ramanathan, V., Wu, G., Ding, Y., Manoj, M. G., Liu, J., Qian,  
582 Y., Li, J., Zhou, T., Fan, J., Rosenfeld, D., Ming, Y., Wang, Y., Huang, J., Wang, B.,  
583 Xu, X., Lee, S. -S., Cribb, M., Zhang, F., Yang, X., Zhao, C., Takemura, T., Wang,  
584 K., Xia, X., Yin, Y., Zhang, H., Guo, J., Zhai, P. M., Sugimoto, N., Babu, S. S., and  
585 Brasseur, G. P.: Aerosol and monsoon climate interactions over Asia, *Rev. Geophys.*,  
586 866–929, <https://doi.org/10.1002/2015RG000500>, 2016.

587 Liu, F., Beirle, S., Zhang, Q., Dörner, S., He, K., and Wagner, T.: NO<sub>x</sub> lifetimes and  
588 emissions of cities and power plants in polluted background estimated by satellite  
589 observations, *Atmos. Chem. Phys.*, 16, 5283–5298, [https://doi.org/10.5194/acp-16-](https://doi.org/10.5194/acp-16-5283-2016)  
590 [5283-2016](https://doi.org/10.5194/acp-16-5283-2016), 2016.

591 Liu, X., Ma, P. -L., Wang, H., Tilmes, S., Singh, B., Easter, R. C., Ghan, S. J., and Rasch,  
592 P. J.: Description and evaluation of a new four-mode version of the Modal Aerosol

593 Module (MAM4) within version 5.3 of the Community Atmosphere Model, *Geosci.*  
594 *Model Dev.*, 9, 505–522, <https://doi.org/10.5194/gmd-9-505-2016>, 2016.

595 Mahmood, R. and Li, S.: Remote influence of South Asian black carbon aerosol on East  
596 Asian summer climate, *Int. J. Climatol.*, 34, 36–48,  
597 <https://doi.org/10.1002/joc.3664>, 2014.

598 Mu, J., and Wang, Z.: Responses of the East Asian summer monsoon to aerosol forcing  
599 in CMIP5 models: The role of upper-tropospheric temperature change, *Int. J.*  
600 *Climatol.*, 41, 1555–1570, <https://doi.org/10.1002/joc.6887>, 2020.

601 Ramachandran, S., Rupakheti, M., and Lawrence, M. G.: Black carbon dominates the  
602 aerosol absorption over the Indo-Gangetic Plain and the Himalayan foothills,  
603 *Environ. Int.*, 142, 105814, <https://doi.org/10.1016/j.envint.2020.105814>, 2020.

604 Ramachandran, S., Rupakheti, M., Cherian, R.: Insights into recent aerosol trends over  
605 Asia from observations and CMIP6 simulations, *Sci. Total Environ.*, 807, 150756,  
606 <https://doi.org/10.1016/j.scitotenv.2021.150756>, 2021.

607 Ren, L., Yang, Y., Wang, H., Wang, P., Chen, L., Zhu, J., and Liao, H.: Aerosol transport  
608 pathways and source attribution in China during the COVID-19 outbreak, *Atmos.*  
609 *Chem. Phys.*, 21, 15431–15445, <https://doi.org/10.5194/acp-21-15431-2021>, 2021.

610 Samset, B. H., Lund, M. T., Bollasina, M., Myhre, G., and Wilcox, L.: Emerging Asian  
611 aerosol patterns, *Nat. Geosci.*, 12, 582–584, [https://doi.org/10.1038/s41561-019-](https://doi.org/10.1038/s41561-019-0424-5)  
612 [0424-5](https://doi.org/10.1038/s41561-019-0424-5), 2019.

613 Smith, C. J., Kramer, R. J., Myhre, G., Alterskjær, K., Collins, W., Sima, A., Boucher,  
614 O., Dufresne, J.-L., Nabat, P., Michou, M., Yukimoto, S., Cole, J., Paynter, D.,  
615 Shiogama, H., O'Connor, F. M., Robertson, E., Wiltshire, A., Andrews, T., Hannay,  
616 C., Miller, R., Nazarenko, L., Kirkevåg, A., Olivié, D., Fiedler, S., Lewinschal, A.,  
617 Mackallah, C., Dix, M., Pincus, R., and Forster, P. M.: Effective radiative forcing  
618 and adjustments in CMIP6 models, *Atmos. Chem. Phys.*, 20, 9591–9618,  
619 <https://doi.org/10.5194/acp-20-9591-2020>, 2020.

620 Sun, X., Chen, L., and He, J.: Index of land-sea thermal difference and its relation to  
621 interannual variation of summer circulation and rainfall over East Asia, *Acta*  
622 *Meteorol. Sin.*, 60, 164–172, <https://doi.org/10.11676/qxxb2002.020>, 2002 (in  
623 Chinese).

624 Tian, F., Dong, B., Robson, J., and Sutton, R.: Forced decadal changes in the East Asian  
625 summer monsoon: the roles of greenhouse gases and anthropogenic aerosols, *Clim.*  
626 *Dyn.*, 51, 3699–3715, <https://doi.org/10.1007/s00382-018-4105-7>, 2018.

627 van Marle, M. J. E., Kloster, S., Magi, B. I., Marlon, J. R., Daniau, A.-L., Field, R. D.,  
628 Arneeth, A., Forrest, M., Hantson, S., Kehrwald, N. M., Knorr, W., Lasslop, G., Li,  
629 F., Man-geon, S., Yue, C., Kaiser, J. W., and van der Werf, G. R.: Historic global  
630 biomass burning emissions for CMIP6 (BB4CMIP) based on merging satellite  
631 observations with proxies and fire models (1750–2015), *Geosci. Model Dev.*, 10,  
632 3329–3357, <https://doi.org/10.5194/gmd-10-3329-2017>, 2017.

633 Wan, J.-H, Mahmood, R. and Li, S.: Impact of European black carbon on East Asian  
634 summer climate, *Atmos. Oceanic. Sci. Lett.*, 6, 375–380,  
635 <https://doi.org/10.3878/j.issn.1674-2834.13.0037>, 2013.

636 Wang, B., Xiang, B., and Lee, J.-Y.: Subtropical high predictability establishes a  
637 promising way for monsoon and tropical storm predictions, *P. Natl. Acad. Sci.*  
638 *U.S.A.*, 110, 2718–2722, <https://doi.org/10.1073/pnas.1214626110>, 2013.

639 Wang, Z., Lin, L., Xu, Y., Che, H., Zhang, X., Dong, W., Wang, C., Gui, K., and Xie,  
640 B.: Incorrect Asian aerosols affecting the attribution and projection of regional  
641 climate change in CMIP6 models, *Np. J. Clim. Atmos. Sci.*, 4, 1–8,  
642 <https://doi.org/10.1038/s41612-020-00159-2>, 2021.

643 Wu, A., and Ni., Y., The influence of tibetan plateau on the interannual variability of  
644 Asian monsoon, *Adv. Atmos. Sci.*, 14, 491–504, [https://doi.org/10.1007/s00376-](https://doi.org/10.1007/s00376-997-0067-0)  
645 [997-0067-0](https://doi.org/10.1007/s00376-997-0067-0), 1997.

646 Xie, X., Wang, H., Liu, X., Li, J., Wang, Z., and Liu, Y.: Distinct effects of  
647 anthropogenic aerosols on the East Asian summer monsoon between multidecadal  
648 strong and weak monsoon stages, *J. Geophys. Res. Atmos.*, 121, 7026–7040,  
649 <https://doi.org/10.1002/2015JD024228>, 2016.

650 Yang, Y., Wang, H., Smith, S. J., Ma, P.-L., and Rasch, P. J.: Source attribution of black  
651 carbon and its direct radiative forcing in China, *Atmos. Chem. Phys.*, 17, 4319–  
652 4336, <https://doi.org/10.5194/acp-17-4319-2017>, 2017a.

653 Yang, Y., Russell, L. M., Lou, S., Liao, H., Guo, J., Liu, Y., Singh, B., and Ghan, S. J.:  
654 Dust-wind interactions can intensify aerosol pollution over eastern China, *Nat.*  
655 *Commun.*, 8, 15333, <https://doi.org/10.1038/ncomms15333>, 2017b.

656 Yang, Y., Wang, H., Smith, S. J., Easter, R., Ma, P.-L., Qian, Y., Yu, H., Li, C., and  
657 Rasch, P. J.: Global source attribution of sulfate concentration and direct and

658 indirect radiative forcing, *Atmos. Chem. Phys.*, 17, 8903–8922,  
659 <https://doi.org/10.5194/acp-17-8903-2017>, 2017c.

660 Yang, Y., Smith, S. J., Wang, H., Mills, C. M., and Rasch, P. J.: Variability, timescales,  
661 and nonlinearity in climate responses to black carbon emissions, *Atmos. Chem.*  
662 *Phys.*, 19, 2405–2420, <https://doi.org/10.5194/acp-19-2405-2019>, 2019.

663 Yang, Y., Ren, L., Li, H., Wang, H., Wang, P., Chen, L., Yue, X., and Hong, L.: Fast  
664 climate responses to aerosol emission reductions during the COVID-19 pandemic,  
665 *Geophys. Res. Lett.*, 47, e2020GL089788, <https://doi.org/10.1029/2020GL089788>,  
666 2020.

667 Yang, Y., Ren, L., Wu, M., Wang, H., Song, F., Leung, L. R., Hao, X., Li, J., Chen, L.,  
668 Li, H., Zeng, L., Zhou, Y., Wang, P., Liao, H., Wang, J., and Zhou, Z.-Q.: Abrupt  
669 emissions reductions during COVID-19 contributed to record summer rainfall in  
670 China, *Nat. Commun.*, 13, 959, <https://doi.org/10.1038/s41467-022-28537-9>, 2022.

671 Yu, H., Chin, M., West, J. J., Atherton, C. S., Bellouin, N., Bergmann, D., Bey, I., Bian,  
672 H., Diehl, T., Forberth, G., Hess, P., Schulz, M., Shindell, D., Takemura, T., and Tan,  
673 Q.: A multimodel assessment of the influence of regional anthropogenic emission  
674 reductions on aerosol direct radiative forcing and the role of intercontinental  
675 transport, *J. Geophys. Res. Atmos.*, 118, 700–720,  
676 <https://doi.org/10.1029/2012jd018148>, 2013.

677 Zeng, L., Yang, Y., Wang, H., Wang, J., Li, J., Ren, L., Li, H., Zhou, Y., Wang, P., and  
678 Liao, H.: Intensified modulation of winter aerosol pollution in China by El Niño  
679 with short duration, *Atmos. Chem. Phys.*, 21, 10745–10761,  
680 <https://doi.org/10.5194/acp-21-10745-2021>, 2021.

681 Zhang, H., Wang, Z., Wang, Z., Liu, Q., Gong, S., Zhang, X., Shen, Z., Lu, P., Wei, X.,  
682 Che, H., and Li, L.: Simulation of direct radiative forcing of aerosols and their  
683 effects on East Asian climate using an interactive AGCM-aerosol coupled system,  
684 *Clim. Dyn.*, 38, 1675–1693, <https://doi.org/10.1007/s00382-011-1131-0>, 2011.

685 Zhang, X. Y., Wang, Y. Q., Niu, T., Zhang, X. C., Gong, S. L., Zhang, Y. M., and Sun,  
686 J. Y.: Atmospheric aerosol compositions in China: spatial/temporal variability,  
687 chemical signature, regional haze distribution and comparisons with global aerosols,  
688 *Atmos. Chem. Phys.*, 12, 779–799, <https://doi.org/10.5194/acp-12-779-2012>, 2012.

689 Zhang, Z., Guan, H., Luo, L., Zheng, N., and Xiao, H.: Response of fine aerosol nitrate  
690 chemistry to Clean Air Action in winter Beijing: Insights from the oxygen isotope

691 signatures, Sci. Total Environ., 746, 141210,  
692 <https://doi.org/10.1016/J.SCITOTENV.2020.141210>, 2020.  
693 Zheng, B., Tong, D., Li, M., Liu, F., Hong, C., Geng, G., Li, H., Li, X., Peng, L., Qi, J.,  
694 Yan, L., Zhang, Y., Zhao, H., Zheng, Y., He, K. and Zhang, Q.: Trends in China's  
695 anthropogenic emissions since 2010 as the consequence of clean air actions, Atmos.  
696 Chem. Phys., 18, 14095–14111, <https://doi.org/10.5194/acp-18-14095-2018>, 2018.  
697